Climate Dynamics (1997) 13: 821–834

Climate Dynamics

Radiative forcing and response of a GCM to ice age boundary conditions: cloud feedback and climate sensitivity

C. D. Hewitt, J. F. B. Mitchell

Hadley Centre for Climate Prediction and Research, Meteorological Office, London Road, Bracknell, RG12 2SY, UK

Received: 8 February 1997 / Accepted: 4 June 1997

Abstract. A general circulation model is used to examine the effects of reduced atmospheric CO_2, insolation changes and an updated reconstruction of the continental ice sheets at the Last Glacial Maximum (LGM). A set of experiments is performed to estimate the radiative forcing from each of the boundary conditions. These calculations are used to estimate a total radiative forcing for the climate of the LGM. The response of the general circulation model to the forcing from each of the changed boundary conditions is then investigated. About two-thirds of the simulated glacial cooling is due to the presence of the continental ice sheets. The effect of the cloud feedback is substantially modified where there are large changes to surface albedo. Finally, the climate sensitivity is estimated based on the global mean LGM radiative forcing and temperature response, and is compared to the climate sensitivity calculated from equilibrium experiments with atmospheric CO_2 doubled from present day concentration. The calculations here using the model and palaeodata support a climate sensitivity of about $1\ Wm^{-2}K^{-1}$ which is within the conventional range.

1 Introduction

The Last Glacial Maximum (LGM), about 21 000 years before present (21 kBP), represents the largest climate change of recent geologic times. A wealth of palaeoclimatic data has provided reconstructions of the state of the Earth's surface, the sea surface, and the atmospheric composition of trace gases and aerosols at this period (e.g., CLIMAP Project Members 1981; COHMAP members 1988). As a result the LGM has been the subject of several general circulation model (GCM) studies to test the ability of GCMs to simulate a climate regime very different from the present (e.g., Gates 1976; Hansen et al. 1984; Manabe and Broccoli 1985a, b; Kutzbach and Guetter 1986; Broccoli and Manabe 1987; Lautenschlager and Herterich 1990) by specifying various boundary conditions appropriate for the Ice Age Earth. By assessing the ability of GCMs to simulate such changes of climate we can hope to assess their reliability at simulating future climates.

In particular, simulations of the LGM can be used to estimate the sensitivity of climate to radiative forcing. This is a major uncertainty in the prediction of future climate change due to anthropogenic emissions (Houghton et al. 1995). It is difficult to estimate climate sensitivity from the instrumental temperature record over the last century because of uncertainties in climate forcing, the rate of uptake of heat by the ocean, and the contribution from natural climate variability. The estimated change in radiative forcing from 21 kBP is much larger than from the pre-industrial period, and the assumption of quasi-equilibrium of the 21 kBP climate avoids the uncertainty in the rate of heat uptake from the ocean, so in principle, the changes from 21 kBP give a better opportunity to estimate climate sensitivity. The simulations can be used either to estimate the forcing at 21 kBP, and then utilise the reconstructed temperatures to derive the sensitivity, or the model simulations can be used to derive the climate sensitivity directly. In this study we adopt both approaches using results from several models.

Previous studies by Hansen et al. (1993) and Hoffert and Covey (1992) used the reconstructions to infer the radiative forcing and temperature change at the LGM and hence the equilibrium climate sensitivity. They then used this and an estimate of the radiative forcing due to doubling CO_2 to infer a global mean future equilibrium temperature change. Manabe and Broccoli (1985a) compared two versions of the GFDL model, one with a fixed cloud distribution and the other with a parametrisation to predict cloud, to assess which cloud scheme produced a realistic climate change simulation of the LGM. Both of these schemes have been used in experiments simulating the climate response to a doubling of CO_2.

The UKMO Hadley Centre model is described in Sect. 2 along with the design of the GCM experiments. A climate model essentially converts a forcing (described in Sect. 3) into a response (described in Sect. 4). Feedbacks

Correspondence to: C. Hewitt
E-mail: cdhewitt@meto.gov.uk

in the climate system modify the basic forcing–response relationship. Here the sea ice and cloud feedbacks are investigated by quantifying the radiative impact of changes in the sea–ice cover and cloud simulated by the model. The climate sensitivity, as estimated from the ratio of the forcing to the response both from the GCM and from palaeoclimatic reconstructions, is examined in Sect. 5.

2 The model and experimental design

2.1 The model

The UKMO atmospheric climate model is coupled to a mixed layer ocean model and a sea ice model, all at a horizontal grid-resolution of 2.5° by 3.75° and is henceforth referred to as HADSM2b. The atmospheric model is version HADAM2b of the UKMO unified forecast and climate model (Cullen 1993), which is similar to version HADAM2 described in Hewitt and Mitchell (1996a) and has 19 levels on hybrid vertical coordinates (Simmons and Burridge 1981) with terrain-following sigma coordinates (sigma = pressure/surface pressure) in the bottom four layers, pressure coordinates for the top three layers, and a linear combination for the intermediate 12 layers. The changes made to the atmospheric model physics between these two versions are described in Hall et al. (1995). The main differences are a modification of the temperature range of partitioning of mixed-phase clouds (clouds which contain both liquid and frozen water) from 0° to −15 °C in HADAM2 to 0° to −9 °C; the gravity wave drag scheme includes anisotropy of the orography, trapped lee waves, and a better representation of flow blocking from high drag states; negative humidities are corrected by borrowing moisture from neighbouring grid-points, and altered coefficients for horizontal diffusion which is used to remove unwanted grid-scale noise and to represent dissipation by unresolved eddies.

The mixed layer ocean model represents the ocean as a 50 m well-mixed layer of water, with a prescribed seasonally varying heat flux H. The rate of change of temperature T of the mixed layer at each grid-point is given by

$$\rho C_P h \frac{\partial T}{\partial t} = H + S \tag{1}$$

where ρ and C_P are the density and specific heat capacity of sea water respectively, and h is the depth of the mixed layer (50 m). S is the net heat flux from the atmosphere, and H accounts for the transfer of heat in the ocean due to ocean dynamics as well as model errors. H is derived from Eq. 1 by diagnosing S from an atmospheric integration where the sea-surface temperatures (SSTs) and sea–ice depth are prescribed using climatological values. Note that the heat flux H applied at each grid-point is the same in the control and anomaly simulations which means that any changes in computed SST are due to changes in S only. Also, more importantly, H is only applied at ocean points in the mixed layer ocean model, and so the lowering of the sea level at the LGM means that there are new land points where values of H are not used. This means that there are no changes to the heat flux at each LGM ocean grid-point, but there is a change to the global mean forcing since some present day ocean points no longer exist. This 'lost heat flux' is quantified in Sect. 3.

The sea–ice model incorporates both the dynamics and thermodynamics of sea-ice, and is essentially the same as that used in the full ocean GCM described in Johns et al. (1997). The thermodynamic properties are based on the zero-dimensional model of Semtner (1976), and leads are represented following Hibler (1979). Sea ice forms when the ocean temperature falls below 271.35 K; the top surface temperature of the ice is calculated by the atmosphere model and the temperature of the mixed layer under the ice is fixed at 271.35 K. A simple parametrisation of sea–ice dynamics is included, based on Bryan (1969), with the ice thickness, ice concentration and snow depth advected using a climatology of ocean surface currents.

2.2 Experimental design

The Paleoclimate Modelling Intercomparison Project (PMIP, Joussaume and Taylor 1995) is coordinating modelling and data reconstruction efforts on two time periods, 6 kBP and 21 kBP. The experimental design of each PMIP GCM simulation, in particular the boundary conditions for the model, has been made as similar as possible to facilitate model–model comparisons.

The PMIP recommended ice age boundary conditions differ from those of the present day by representing a change to the land surface characteristics to include the extensive continental ice sheets and modified coastlines to account for a sea level lowering of about 105 m, lowering the atmospheric composition of greenhouse gases, and a different pattern of insolation arising from a change to the Earth's orbit. Note, however, that the snow-free and ice-free land surface albedos are not changed although new values of albedo are specified for emerged land points resulting from the sea level lowering.

A set of six experiments was run to assess the radiative forcing and response of surface temperature to the 21 kBP boundary conditions (Table 1). A control experiment CON was run to simulate the present day climate. The LGM experiment, to simulate the climate of 21 kBP, incorporates all of the changes to the control experiment described in the following paragraph, and Table 1 lists the changes made for the other four experiments, which help isolate the contribution of individual changes.

The orbital parameters have been calculated from Berger (1978), fixing the vernal equinox at noon on March 21st, and are listed in Table 2 and the resulting insolation changes are illustrated in Fig. 1. Atmospheric CO_2 concentrations have been lowered at 21 kBP by about 29% (the same ratio as other GCM experiments involved in PMIP) from the 323 ppmv used in CON, this gives the same ratio as reducing CO_2 from a pre-industrial concentration of 280 ppmv to an ice age level of 200 ppmv, and therefore the same radiative forcing. The reason for using a forcing relative to pre-industrial times is that the current climate and the modern vegetation have probably not come into equilibrium with the recent rapid rise in CO_2, and a reduction from modern to 21 kBP CO_2 values may be larger than that seen over the period of the data

Table 1. Description of experiments. P refers to present day values, L is for 21 kBP, and for the ALB1 and ALB2 experiments the albedo is either updated every month (mth) or fixed (fix) (see text for further details)

	CON	LGM	TOP	ORB	ALB1	ALB2
Orbital parameters	P	L	P	L	P	P
Atmospheric CO_2	P	L	P	P	P	P
Orography (including ice)	P	L	L	P	P	P
Surface albedo	P	L	L	P	L (fix)	L (mth)
Length of run (in years)	20	20	5	3	2	2
Length of spin-up	10	16	8	1	0	0

Table 2. Orbital parameters for the control (present day) and LGM (21 kBP) experiments derived from Berger (1978)

	0 kBP	21 kBP
Longitude of perihelion (relative to the vernal equinox)	102.5°	114.4°
Obliquity	23.44°	22.95°
Eccentricity	0.0167	0.0190

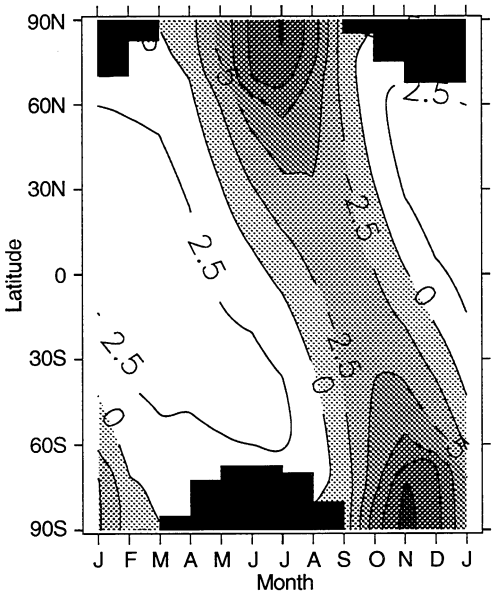

Fig. 1. Time-latitude diagram (zonal average of monthly mean values) of change in incoming shortwave radiation at the top of the atmosphere between 21 kBP and 0 kBP with *areas of decrease shaded*. The polar night has been masked out. Contours every 2.5 Wm^{-2}

reconstructions. The model's land distribution and topography need to be modified at 21 kBP to take into account the lower sea level and the large continental ice sheets that existed at the last glacial maximum. Peltier's ICE-3G 1° by 1° resolution ice sheet reconstruction (Tushingham and Peltier 1991) has been interpolated onto the model's grid. This data provides the extra land points exposed as a result of the sea level lowering, and the orographic heights of the ice sheets. The surface albedo at permanent land ice points is initialised to be 75%, but this can increase to up to 80% with snow cover. The albedo of the ice-free land grid-points exposed by the lowering of sea level is set to the zonal mean value, averaged over all snow- and ice-free land grid-points, located at that same latitude. The surface albedos of all other points are set as in CON. The solar constant is kept fixed at 1365 Wm^{-2} in all of the experiments.

TOP includes the 21 kBP topography and surface albedo, both of which are dominated by the presence of the ice age ice-sheets. ORB isolates the effect of the 21 kBP orbital parameters. ALB1 and ALB2 are the same experiment as the control but the solar radiation code is called twice, once with the present-day surface albedos and then with the 21 kBP surface albedos, to determine the radiative forcing due to 21 kBP surface albedos. ALB2 has the surface albedos for 21 kBP updated every month, with the albedos determined from monthly means of the LGM experiment. The ALB1 experiment uses the same surface albedo data that was used to initialise the LGM experiment, does not vary throughout the year, uses snow-free land surface albedos (i.e., 75% over the ice sheets) and hence does not include any of the feedbacks that may have operated in the LGM experiment, in particular the effect of higher albedo snow cover and more extensive sea ice.

The initial years ("length of spin-up" in Table 1) of the CON, LGM, TOP, and ORB experiments are ignored to allow the atmosphere-mixed layer ocean-sea ice coupled climate system to adjust to the forcings and reach quasi-equilibrium. The "spin-up" phase for the LGM experiment needs to be longer due to the revised boundary conditions and lowering of CO_2, while the TOP spin-up period is shorter since only the 21 kBP orography and albedo are introduced. Results presented in the following section are averages over the length of the run, as listed in Table 1.

3 Radiative forcing of the climate system due to 21 kBP boundary conditions

To help analyse the sensitivity of the GCM to radiative forcing, we use a zero-dimensional energy balance model approach (for example, Dickinson 1986), using globally averaged quantities from the GCM. The change in temperature ΔT from equilibrium due to a heating perturbation (radiative forcing) ΔQ is given by the thermodynamic equation

$$C\frac{\partial \Delta T}{\partial t} + \lambda \Delta T = \Delta Q \tag{2}$$

where C is the heat capacity of the system ($= \rho C_P h$, as in Eq. 1) and λ is an inverse measure of the overall sensitivity

of the climate system, to be discussed in Sect. 5. The solution of this equation, for an instantaneous "switch on" of ΔQ is

$$\Delta T = \frac{\Delta Q}{\lambda(1 - e^{-t/\tau})} \quad (3)$$

where $\tau = \frac{C}{\lambda}$ represents the e-folding time of the response of the climate system. At equilibrium $\lambda = \frac{\Delta Q}{\Delta T_{EQ}}$, where ΔT_{EQ} is the equilibrium temperature change. This model with a 50 m mixed layer has an e-folding response time of about 5.4 y (using values of ΔQ and ΔT_{EQ} as listed later in Sects. 3.2 and 4.2 for a doubling of CO_2), hence the need for the long "spin up" time for the LGM experiment listed in Table 1. In the following sections a negative radiative forcing will refer to a forcing that would tend to cool the climate system, and all quantities have been averaged over the full annual cycle.

Table 3. Radiative forcing (Wm^{-2}) deduced from GCM experiments. The rows in bold indicate the forcings that make up the "total" forcing also shown in Fig. 2d

	Global	N. Hemisphere	S. Hemisphere
ALB1: all points	− 2.8	− 4.9	− 0.7
continental ice points only	− 2.3	− 4.3	− 0.2
sea ice points only	0.0	0.0	0.0
ice-free points only	− 0.5	− 0.6	− 0.4
ALB2: all points	− 4.3	− 6.8	− 1.7
continental ice points only	**− 2.9**	**− 5.0**	**− 0.7**
sea ice points only	− 0.8	− 1.0	− 0.6
ice-free points only	**− 0.6**	**− 0.8**	**− 0.4**
Insolation and planetary albedo	**0.1**	**0.1**	**0.1**
Heat convergence	0.6	0.7	0.6
CO_2 estimate	**− 1.7**	**− 1.7**	**− 1.7**
Total	**− 5.1**	**− 7.4**	**− 2.7**

3.1 Surface albedo

ALB1 and ALB2 provide a lower and upper bound on the radiative forcing produced by changes in surface albedo in the LGM experiment. ALB1 uses the surface albedo that the LGM experiment is initialised with, in particular an albedo of 75% as prescribed for bare ice over the continental ice-sheets, and so calculates the initial radiative forcing due to albedo changes. However, in LGM, snow cover accumulates over large regions of the continental ice-sheets, further increasing the surface albedo, and sea ice extents increase. The ALB2 experiment represents the radiative forcing including changes due to high albedo snow accumulating on the ice sheets and the growth of sea ice. This should we hope be a more realistic representation of the ice age surface but is dependent on the model's response to the initial forcing calculated from the ALB1 simulation, and as such represents a climate feedback. The increased surface albedo over the high-latitude oceans is dependent on the sea–ice model and so in the following sections the sea ice forcing is considered as a climate feedback and is not included in the total LGM radiative forcing described later. However, the increased forcing arising from the presence of snow cover on the continental ice-sheets in the context of these experiments is regarded as part of the ice sheet forcing and so it is included in the total LGM radiative forcing later.

The global mean radiative forcing produced using the initial LGM surface albedos (ALB1) is $-2.8\ Wm^{-2}$ (Table 3), and its distribution is similar to that calculated from ALB2 described later, i.e. the largest forcing comes from the continental ice, and is in the Northern Hemisphere. Note that the method used here for calculating the forcing due to albedo changes does not include the effect of the topographic changes, higher ice will have more sunlight impinging on it than the lower land did because of less water vapour absorption. The radiative forcing produced by all the simulated changes in surface albedo (ALB2) in the LGM experiment is $-4.3\ Wm^{-2}$ (Fig. 2a). Globally, most of this forcing is due to the continental ice sheets ($-2.9\ Wm^{-2}$), and occurs in the Northern Hemisphere. There is also an additional forcing of $-0.6\ Wm^{-2}$ brought about by an increase in albedo at grid points that change from ocean to land. The simulated increased glacial sea ice extent (described in Sect. 4) produces a radiative perturbation of $-0.8\ Wm^{-2}$, but for reasons stated above this is treated as a climate feedback.

The studies by Hansen et al. (1993) and Hoffert and Covey (1992) used an older ice-sheet reconstruction (CLIMAP Project Members 1981) which had thicker and higher ice sheets, but an ice albedo of 70%, which is slightly lower than that used in ALB1 and ALB2. Hansen et al. (1993) estimate the radiative forcing due to ice sheets and vegetation to be $-3.5 \pm 1\ Wm^{-2}$, while Hoffert and Covey (1992) estimate the forcing to be $-3.0 \pm 0.5\ Wm^{-2}$. Both of these studies included changes to vegetation which increased the surface albedo. Hansen et al. (1993) used the Köppen scheme to infer vegetation using results taken from a GCM simulation of the climate of the LGM, and these vegetation changes contributed a radiative forcing of about $-0.9\ Wm^{-2}$ (from Hansen et al. 1984). Hoffert and Covey (1992) used the CLIMAP vegetation, and Broccoli and Manabe (1987) used a GCM to calculate the radiative forcing due to imposing this CLIMAP vegetation at the LGM, giving a global mean radiative forcing of about $-0.7\ Wm^{-2}$. It is worth noting that Broccoli and Manabe (1987) state that even though this represents a fairly large forcing, the temperature response to the vegetation change was relatively small (about -0.3 K averaged over all points free of LGM continental ice) when compared to the changes resulting from expanded continental ice-sheets and lowered CO_2. They proposed that this was a consequence of the geographical distribution of the forcings and high-latitude snow and sea–ice feedbacks.

The radiative forcing due to the continental ice sheets from the above estimates are therefore similar to those from the ALB1 and ALB2 experiments (see Table 4) even though the HADSM2b GCM experiments use a different ice-sheet reconstruction and have higher ice albedos. Hansen et al. (1993) calculate a slightly larger forcing (-0.9) from snow-free land albedo changes compared to both the value calculated by Broccoli and Manabe from the

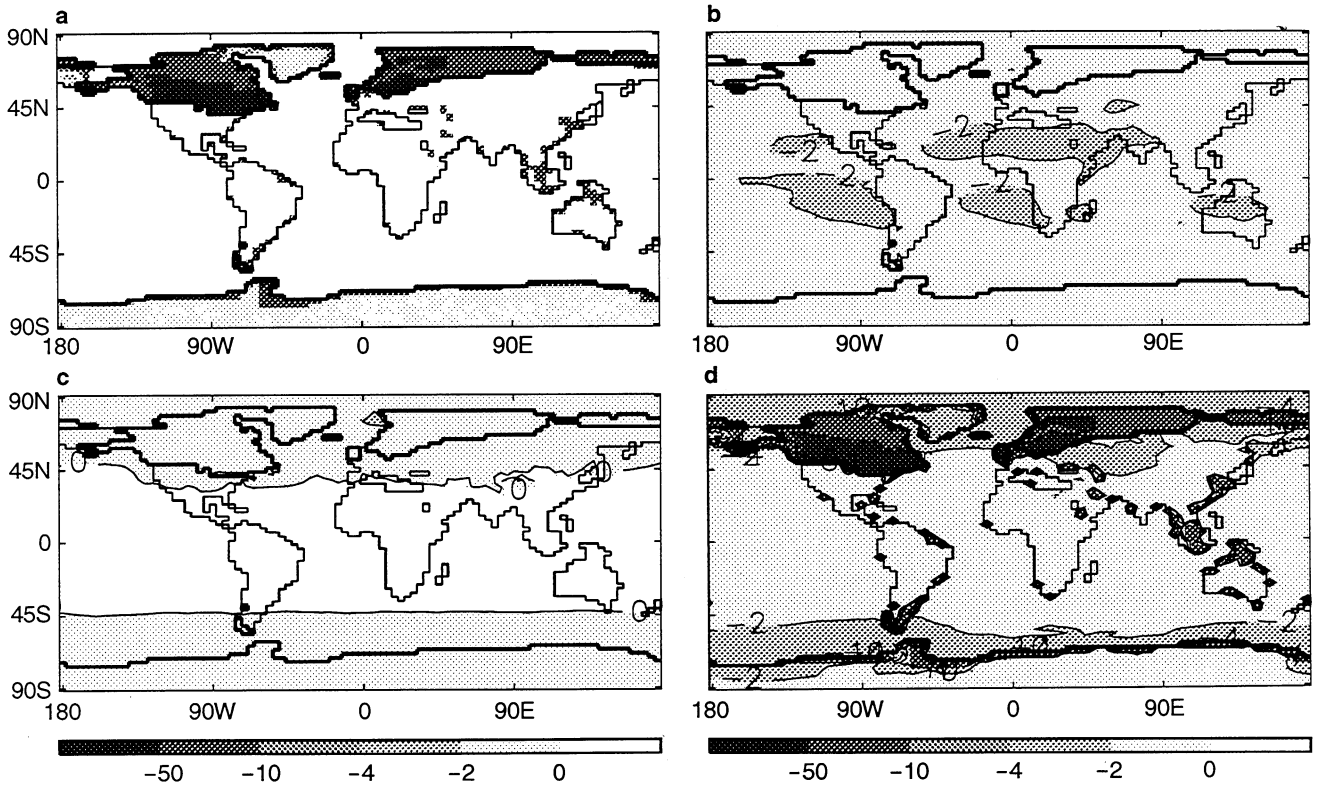

Fig. 2a–d. Change in annual average radiative forcing between 21 kBP and 0 kBP. Contours at -50, -10, -4, -2, 0 Wm^{-2}, *LGM* model coastlines are *marked*, and *thick lines* show position of *LGM* ice sheets. **a** Forcing from experiment ALB2 excluding the sea ice forcing. **b** CO_2 forcing estimated by scaling the forcing from the HADCM2 $2 \times CO_2$ experiment. **c** Forcing from the monthly insolation changes interacting with their albedo changes. **d** Sum of **a**, **b** and **c**

CLIMAP vegetation (-0.7) as used by Hoffert and Covey and the value resulting from ocean points changing to land points in the ALB1 (-0.5) and ALB2 (-0.6) experiments.

3.2 Lower CO_2

The effective forcing of the troposphere, ΔF, due to doubling CO_2 before any climate feedbacks have acted, but allowing for the stratosphere to adjust (Schneider 1975), has been calculated as 3.5 Wm^{-2} using the Hadley Centre coupled ocean-atmosphere model HADCM2 (Mitchell et al. 1995). This forcing can be taken to be proportional to the logarithm of the change in CO_2, i.e.,

$$\Delta F = \chi \ln \frac{C}{C_0} \tag{4}$$

so χ will be $\frac{3.5}{\ln 2}$ ($= 5.0$), and we can use this value as a best guess for this mixed layer ocean model. This implies that the forcing due to a 29% reduction in CO_2 would be -1.7 Wm^{-2} and Fig. 2b shows the forcing due to doubling CO_2 scaled accordingly (Johns, personal communication).

Hansen et al. (1993) estimated the forcing during the LGM relative to the Holocene due to three greenhouse gases (CO_2, CH_4, N_2O) to be -2.6 ± 0.5 Wm^{-2}, and Hoffert and Covey (1992) estimated the forcing due to CO_2 and CH_4 to be -2.8 ± 0.3 Wm^{-2}. These estimates are larger than that from HADSM2b because of the forcing from the additional greenhouse gases and the use of a higher value for χ in Eq. 4. The CO_2 forcing in the Hansen et al. (1993) study is -2.1 Wm^{-2} and in the Hoffert and Covey (1992) study is -2.3 Wm^{-2} with a forcing from the additional greenhouse gases of about -0.5 Wm^{-2}. Repeating the CO_2 forcing calculations with a value of $\chi = 5.0$ in Eq. 4 produces values more in line with the -1.7 Wm^{-2} reported above (see Table 4). A total greenhouse gas forcing based on the above would be of the order of -2.2 Wm^{-2}.

3.3 Insolation

The global mean radiative forcing due to insolation changes can be estimated by calculating $\Delta S(1 - \alpha_P)$, where ΔS is the change in annual mean insolation and α_P is the annual global mean present day planetary albedo. This

Table 4. LGM radiative forcing ΔQ_{LGM} (Wm^{-2}), temperature change ΔT_{LGM} (K), and implied climate sensitivity λ_{LGM} ($Wm^{-2}K^{-1}$), and radiative forcing $\Delta Q_{2\times CO_2}$ and temperature change $\Delta T_{2\times CO_2}$ resulting from doubling atmospheric CO_2 concentrations from present values, deduced from this work and other studies

		This study	Hansen et al. (1993)	Hoffert and Covey (1992)	Broccoli and Manabe (1987)
ΔQ_{LGM}	Ice sheet	−2.9	−2.6	−2.3	−0.9[a,b]
	Vegetation		−0.9	−0.7	−0.7
	Surface albedo	−0.6			
	CO_2	−1.7[c]	−1.6[c]	−1.8[c]	−1.3[a] (−2.0)[c]
	Additional trace gas forcing		−1.0	−1.0	
	Insolation	0.1			
	Aerosols		−1.0	−0.9	
	Total	−5.1	−7.1	−6.7	−2.9
ΔT_{LGM}		−4.9	−5.0	−3.0	−3.6
λ_{LGM}	implied from proxy data		1.4	2.2	
	implied from GCM	1.0			0.8
$\Delta Q_{2\times CO_2}$		3.5[c]	4.2	4.4	3.5[c]
$\Delta T_{2\times CO_2}$	implied from above	3.4	3.0	2.0	4.3[d]
	GCM simulated	2.9			2.3[e]

[a] This is the published estimate based on a simple calculation for radiative forcing
[b] A revised estimate with the PMIP ice sheet, surface albedo change and a new radiation scheme gives a combined ice sheet and surface albedo forcing of $-2.3\ Wm^{-2}$ (Broccoli, personal communication)
[c] This is based on a value of $3.5\ Wm^{-2}$ for the effective forcing at the tropopause due to doubling CO_2 concentrations from present day values before any climate feedbacks have acted, but allowing for the stratosphere to adjust, using HADCM2 (Mitchell et al. 1995)
[d] If the revised estimates ofthe LGM forcings are used this gives an implied sensitivity to doubling CO_2 of 2.9 K which is more consistent with the results here
[e] As reported in Manabe and Broccoli (1985a)

gives a radiative forcing very close to zero. However, a more accurate insolation forcing can be calculated by considering the seasonal and latitudinal pattern of insolation changes interacting with the seasonal and latitudinal variation of present-day planetary albedo (as used in ALB2). The forcing calculated this way, using monthly mean values for insolation and albedo, is larger, but still only amounts to about $0.1\ Wm^{-2}$, which is small when compared to the forcings described previously, but of the opposite sign. The reduced tilt of the Earth's axis redistributes the insolation to the darker low latitudes, which outweighs the summer insolation decreases over the relatively small high latitudes where the albedo is large (Fig. 2c).

3.4 'Lost heat flux'

The global mean surface heat flux (H in Eq. 1) in the control simulation is $-2.8\ Wm^{-2}$. In the simulations with 21 kBP land-sea distributions (LGM and TOP) the heat flux is $-2.2\ Wm^{-2}$, implying that the heat flux that is 'lost' as a result of land grid-points becoming ocean grid-points amounts to a global mean radiative forcing of $0.6\ Wm^{-2}$. If this were added to the total forcing described later, the negative forcing in the Barents Sea and Bering Sea would increase in the location of the ice age ice-sheets, and there would be a positive forcing around Malaysia and Indonesia. In an experiment parallel to the LGM experiment, in which this heat flux is distributed equally over all LGM ocean points so that the global mean H is the same as in CON, the climatology is similar to the LGM experiment with similar patterns of temperature change, but the annual mean cooling is 0.5 K more than in the LGM experiment. This 'lost heat flux' will not be included in the total LGM radiative forcing calculations that follow, but it does influence the response described in Sect. 4.

3.5 Total forcing estimate

The total radiative forcing at the LGM, using the CLIMAP ice sheet reconstruction, is estimated to be $-7.1 \pm 1.5\ Wm^{-2}$ by Hansen et al. (1993) and $-6.7 \pm 0.9\ Wm^{-2}$ by Hoffert and Covey (1992). However, both these studies include the radiative forcing of increased glacial atmospheric aerosols, which they estimate to be about $-1 \pm 0.5\ Wm^{-2}$, have a relatively large greenhouse gas forcing as mentioned already, and include the forcing from higher ice age surface albedos resulting from vegetation changes. If we take into account their estimate of the radiative forcing due to ice age atmospheric aerosol loading, the forcing from additional greenhouse gas changes, and Broccoli and Manabe's (1987) estimate of vegetation forcing, the best guess of the total global climate forcing during the ice age, relative to the Holocene climate, based on the GCM experiments reported here would be of the order of $-6.5\ Wm^{-2}$.

The estimated geographical pattern of the radiative forcing in the LGM experiment is shown in Fig. 2d. This represents the sum of the forcing from ALB2 (excluding the sea–ice changes), the insolation forcing interacting with the albedo changes, and a forcing due to lowered CO_2 concentrations calculated by scaling the forcing derived from experiments with doubled CO_2 using HADCM2, and has a global average of $-5.1\ Wm^{-2}$. In summary, there is a large negative forcing due to the inclusion of the Northern Hemisphere ice-sheets with local values in excess of $-50\ Wm^{-2}$, a large negative forcing due to lowered CO_2 concentrations, a fairly large negative forcing over new land points whose albedo has increased from the dark ocean to brighter vegetation with values exceeding $-10\ Wm^{-2}$ locally, and a relatively small zonal pattern produced by the insolation changes with a negative forcing at high latitudes and a positive forcing throughout the subtropics and Tropics.

4 Response of the climate system to LGM boundary conditions

4.1 Simulated LGM climate

The global mean cooling simulated at the LGM by HADSM2b, is 4.4 K. This is in line with other GCM simulations (see Hewitt and Mitchell 1996b for a summary of some PMIP simulations) and estimates from proxy records (e.g. the 5 K quoted by Hansen et al. 1993). Table 5 summarises the contribution from each of the changed boundary conditions to this total cooling, and these contributions are described in more detail in the following section. The largest temperature changes occur over land and in the Northern Hemisphere, with maxima over the ice sheets (Fig. 3a), consistent with the radiative forcing described previously. However, as has been reported in the previous section, the LGM experiment does not include the effect of glacial aerosols, additional greenhouse gases and vegetation changes.

The high-latitude near-surface air temperature changes described earlier produce dramatic changes in the thickness and extent of sea ice. The Southern Hemisphere sea ice becomes thicker (by about 1 m), with the sea–ice edge extending further equatorward, particularly in winter, though not as far as indicated by the CLIMAP data. The Northern Hemisphere sea–ice changes simulated at the LGM are much larger than those of the Southern Hemisphere. Most of the Arctic becomes permanently covered throughout the year with depths exceeding 15 m, an increase of typically 10 m compared to the control. A large region of the northwestern Pacific becomes partially ice covered in winter, extending equatorwards to about 45 °N, as does the Norwegian Sea and most of the northwestern sector of the North Atlantic, extending equatorwards along the east American coast to about 45 °N. Permanent winter sea–ice is evident over the Labrador Sea and north of Iceland. In summer the permanent sea–ice boundary retreats back to the Davis Strait and the Greenland Sea, although the Norwegian Sea and Labrador Sea remain partially ice covered.

The albedo effect of the increased glacial sea–ice cover produces an additional radiative forcing of $-0.8\ Wm^{-2}$ (Table 3) which is about 15% of the size of the total radiative forcing described in Sect. 3, and represents a positive feedback enhancing the cooling from the altered surface boundary conditions. This forcing is larger in the Northern Hemisphere, but it has relatively more effect on the response in the Southern Hemisphere, representing about 22% of the total Southern Hemisphere forcing.

The CLIMAP reconstruction provides global SST data at the LGM against which the GCM can be compared (Fig. 4a). The GCM produces a qualitatively similar pattern to the CLIMAP data, but there are some notable differences, also found in other GCM results. The model cools more than the CLIMAP reconstruction indicates in the Tropics, and less in mid-latitudes. The differences in the Tropics dominate and the modelled global mean cooling is about 0.4 K larger than indicated by the CLIMAP data set. There are much larger regional differences (not shown). This implies one or more of the following:

1. There are inaccuracies in the CLIMAP data set. The low-latitude SSTs have been the subject of much speculation, with some indicators implying a much larger cooling, for example a 5 °C cooling inferred from Barbados corals (Guilderson et al. 1995). Broccoli and Marciniak (1996) performed a comparison of GCM results with CLIMAP data but only used model data at grid-points where sediment cores exist and found that the results analysed in this way agreed much more favourably than a comparison made using the data set subjectively interpolated by the CLIMAP project members. This is also true with this GCM, apart from at high latitudes (Fig. 4b) most noticeably in the Northern Hemisphere although the number of model grid-boxes for which there are sediment cores

Table 5. Annual mean 1.5 m temperature change, in Kelvin, induced by the changed boundary conditions simulated and estimated. Note that the land-sea mask is different at 21 kBP

		Global	N. Hemisphere	S. Hemisphere	Land	Ocean
Total	(simulated)	− 4.4	− 6.5	− 2.3	− 8.1	− 1.7
Topography and surface albedo	(simulated)	− 3.0	− 5.0	− 1.1	− 6.3	− 0.6
CO_2	(estimated)	− 1.4	− 1.6	− 1.2	− 1.8	− 1.2
Insolation	(simulated)	− 0.1	0.1	− 0.2	0.0	− 0.1
Topography	(estimated)	− 0.7	− 1.0	− 0.3	− 1.9	0.0
Total of rows 2, 3, 4		− 4.5	− 6.5	− 2.5	− 8.1	− 1.9

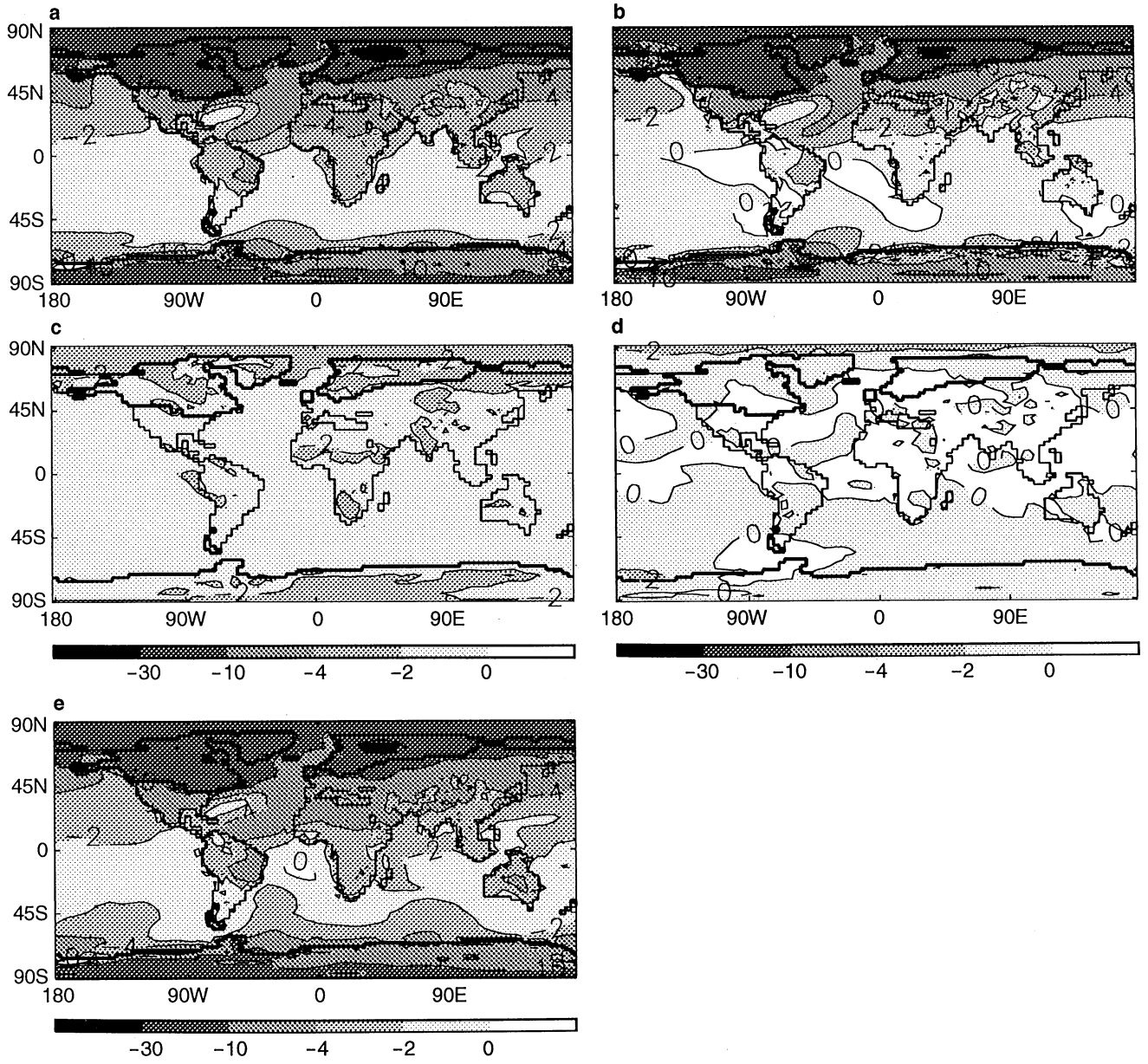

Fig. 3a–e. Change in annual average 1.5 m temperature between 21 kBP and 0 kBP. Contours at -30, -10, -4, -2, 0 K. **a** Experiment LGM. **b** Experiment TOP. **c** Estimated by scaling the temperature change from the HADSM2b $2 \times CO_2$ experiment. **d** Experiment ORB. **e** Sum of TOP, CO_2 estimate, and ORB

to compare to is small. CLIMAP also produces a larger cooling in the Southern Ocean than the GCM, but it has been suggested that CLIMAP overestimated the sea–ice extent there at the LGM (Burckle et al. 1982).

2. The model simulation may be wrong and there may be shortcomings in representing essential components of the climate system, for example, the mixed layer ocean model is not capable of simulating any changes in ocean circulation.

3. The forcing for the LGM climate is incorrect. This may be due to the absence or inaccuracy of a particular component of the total forcing.

4.2 Components of surface temperature response

The previous section has illustrated that the largest radiative forcing in the LGM simulation is the increased surface albedo. It is not possible to isolate the temperature change due to albedo changes in these GCM experiments from the temperature change due to topographic height changes because the changes in elevation will produce changes in the water vapour column. The high-altitude ice will have more sunlight impinging on it than the lower land did, because of less water vapour absorption. This factor is more important than one might think since water

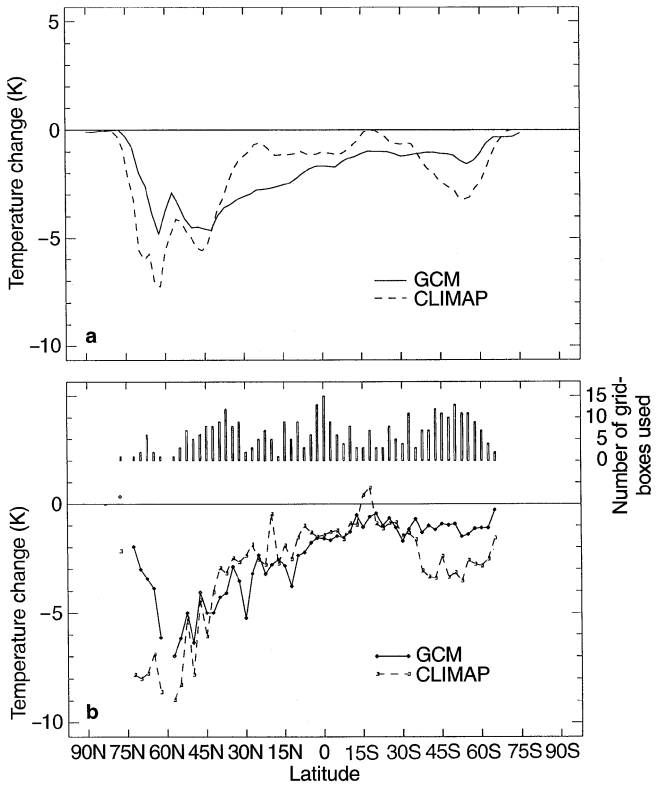

Fig. 4a, b. Zonal mean change in SST between 21 kBP and 0 kBP using the average of February and August SSTs. *Solid line* is GCM, *dashed line* is CLIMAP. **a** Using gridded subjective CLIMAP analysis. **b** Only using GCM grid-boxes where CLIMAP data is located, and a histogram showing the number of such grid-boxes at each latitude

vapour is a strong absorber of solar radiation in the invisible part of the solar spectrum. However, a crude and simple estimate can be made of the cooling that could result from the higher topography alone.

TOP combines the surface albedo changes with the topographic height changes and produces a cooling of 3 K, about two-thirds of the total cooling (Table 5 and Fig. 3b). The global average increase in the model's topographic heights (above mean sea level) is about 100 m, which represents an increase of about 290 m if averaged only over the model's land points. Assuming the environmental lapse rate for the troposphere is 6.5 K per kilometre would imply that the model's global surface air temperature would drop by about 0.65 K due to the model's higher topography (roughly 15% of the total cooling) and over the land the cooling would be about 1.9 K. Therefore, the cooling is not dominated solely by the trivial cooling resulting from increasing the height of the Earth's surface, but rather by the albedo effect of the high-altitude ice. However, the cooling resulting from increasing topography would force more feedbacks which would give a larger cooling, for example the cooling would produce increases in snow cover and sea ice.

The global mean warming simulated on doubling CO_2 using HADSM2b is 2.9 K (Senior, personal communication). This would imply that the lowering of CO_2 at 21 kBP would be expected to produce a cooling of about 1.4 K compared to the control simulation ($\Delta F_{LGM\,CO_2} \times \frac{\Delta T_{2\times CO_2}}{\Delta F_{2\times CO_2}} = -1.7 \times \frac{2.9}{3.5}$), about one-third of the total cooling. Even though the gas is well-mixed in the atmosphere the temperature response would not be uniform (Fig. 3c shows an estimate based on scaling the computed response to doubling CO_2) due to feedbacks in the climate system.

The global average annual mean change in insolation at 21 kBP compared to present-day is close to zero, with relatively small regional and seasonal insolation changes, maximum decreases at the poles of less than 15 Wm^{-2} in the summer hemisphere, due mainly to the decrease in the tilt of the Earth's axis, and changes of less than 5 Wm^{-2} at most other latitudes (Fig. 1). The global average annual mean temperature response to insolation changes is very small, of the order of one-tenth of a degree Kelvin (ORB). Averaged over the full annual cycle there is less insolation at high latitudes and more at low latitudes, which would tend to cool the high latitudes and warm the low latitudes, especially in the Northern Hemisphere where there is more land (Fig. 3d).

The last row of Table 5 shows the sum of the temperature changes from the experiments TOP and ORB and estimated from the lowering of CO_2. These values are very similar to the totals simulated by the LGM experiment (first row of Table 5), suggesting that the total response in the LGM experiment can be considered to be a linear combination of the response to each of the changed boundary conditions. Comparing Figs. 3a and 3e shows that the linear combination produces a remarkably similar pattern of temperature change to that simulated in the LGM experiment with values within one or two degrees at most points.

4.3 Cloud changes, cause and effect

4.3.1 Cloud changes The model simulates a cooling of the entire troposphere at 21 kBP, with a maximum cooling in the lower troposphere at high latitudes especially around the Northern Hemisphere ice sheets and sea ice as stated previously, and the upper tropical troposphere. This increases the tropical lapse rate, the low level pole-equator temperature gradient especially in the Northern Hemisphere, and lowers the tropopause, particularly at high latitudes. As a consequence of the tropospheric cooling, the specific humidity of the entire troposphere is reduced.

The lowered tropopause and colder, drier troposphere leads to a downward displacement of the upper tropospheric stratiform cloud decks (Fig. 5a), a decrease in convective cloud cover in mid- and high-latitudes (Fig. 5b), and a large reduction of the low-level stratiform cloud cover around the cold, dry ice sheets. The increased Northern Hemisphere zonal temperature gradient strengthens the North Atlantic storm tracks which produces an increase in low-level layer cloud (associated with synoptic-scale frontal weather systems) over much of the North Atlantic.

The Northern Hemisphere sub-tropical anticyclones are generally strengthened and the Southern Hemisphere

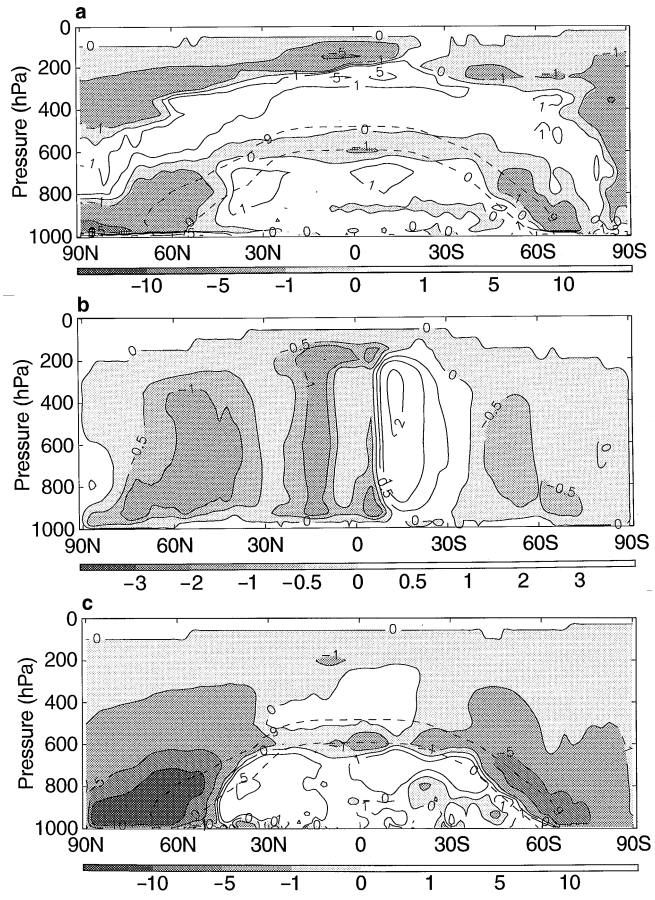

Fig. 5a–c. Zonal mean of annual average changes between 21 kBP and 0 kBP. *Areas of decrease shaded. Dashed lines* show the $-9\,^{\circ}C$ and $0\,^{\circ}C$ from the CON experiment marking the mixed-phase region. The *y-axis* refers to the hybrid vertical coordinate, etc. **a** Layer cloud amount, contours at 0, ± 1, 5, 10%. **b** Convective cloud amount, contours at 0, ± 0.5, 1, 2, 3%. **c** Total cloud water content, contours at 0, ± 1, 5, $10 \times 10^{-6}\,kg^{-1}$

sub-tropical anticyclones are weakened which is accompanied by a weakening and southward displacement of the Inter-Tropical Convergence Zone (ITCZ) especially over northern South America and Central America. This produces a southward displacement of the tropical convective clouds and the upper tropospheric tropical cirrus.

There is also a decrease in cloud in the mixed-phase region of the atmosphere. As the atmosphere cools, more cloud is diagnosed as ice cloud which does not persist for as long as water cloud since the precipitation of cloud ice from cloud is more efficient than for cloud water, and hence the cloud cover is reduced. The radiative properties of the clouds also change, decreases in liquid water fraction and total water content (Fig. 5c) produce a reduction in cloud water path which reduces the albedo and emissivity of the clouds, particularly in mid- and high-latitudes of the Northern Hemisphere.

The importance of changes in the mixed-phase region has been emphasised in experiments with doubled CO_2 concentrations which simulate a warming rather than cooling of the atmosphere (e.g. Senior and Mitchell 1993). The same mechanisms operate, but the changes are of the opposite sign to those reported here.

4.3.2 Cloud feedback The radiative impact of cloud is an important component of the Earth's radiation budget, feedbacks can arise from changes in the height, amount, water content and radiative properties of cloud. Differences in simulated cloud feedback can lead to a factor of two or more difference in climate sensitivity (Senior and Mitchell 1993). Hence it is important to estimate the contribution of clouds to climate sensitivity in the current experiment. A standard measure of cloud feedback is the cloud radiative forcing (see for example Ramanathan et al. 1989), henceforth referred to as CRF. Two diagnostics are used to calculate CRF, the radiative fluxes emitted to space F from an atmosphere including clouds, and the radiative fluxes F_C from a cloud-free atmosphere, which are calculated by calling the model radiation code twice. The radiative impact of adding cloud to a clear-sky earth as seen from space is then $F - F_C$ and so the effect on the planet (with a negative value implying a cooling due to the presence of cloud) is

$$CRF = F_C - F$$

It is instructive to split the CRF into its shortwave ($SW_C - SW$) and longwave ($LW_C - LW$) components (where SW and LW are the outgoing shortwave and long-wave radiation, respectively, and the subscript C refers to clear-sky fluxes of radiation, which are the net fluxes for a cloud-free atmosphere) since clouds tend to cool the climate in the shortwave part of the spectrum, due to reflection mainly from low-level optically thick cloud, and warm the climate in the longwave, due to absorption mainly from high clouds which have a low emitting temperature.

The global mean net cloud radiative forcing at 21 kBP is reduced (i.e becomes less negative) by $1.6\,Wm^{-2}$ (Table 6), mainly as a result of a decrease in shortwave cloud forcing (SCF). The main decreases in SCF are over the ice sheets and where sea ice cover has expanded (Fig. 6a). However, there are several regions where SCF increases, most noticeably in the Northern Hemisphere storm track regions, especially over the North Atlantic, where there is an increase in low-level cloud as discussed already, and northeastern South America and southeastern Asia associated with the southward shift of the ITCZ. The warming effect from the longwave cloud forcing (LCF) is reduced, mainly due to the reduction in high level cloud in the Tropics and over the ice sheets (Fig. 6b). The changes seen in the longwave CRF in the Tropics are consistent with the southward displacement of the ITCZ.

There is a major shortcoming in using change in cloud radiative forcing as a measure of cloud feedback, since cloud forcing can change even if cloud and cloud properties don't. For example, an increase in surface albedo will lead to a bigger increase in the clear-sky solar flux than the cloudy solar flux, and an apparent increase in the solar component of cloud radiative forcing even if cloud hasn't changed. In the 21 kBP experiment, the model simulates large cloud changes in the same regions as the imposed large surface albedo changes, so it is not trivial to separate

Table 6. Changes in global average annual mean cloud forcing (Wm^{-2}) (see text for descriptions of methods)

	ΔLW	ΔSW	Δnet
Method a	− 1.2	2.8	1.6
Method b		2.2	1.0
Method c		0.7	− 0.5
Method d		1.3	0.1

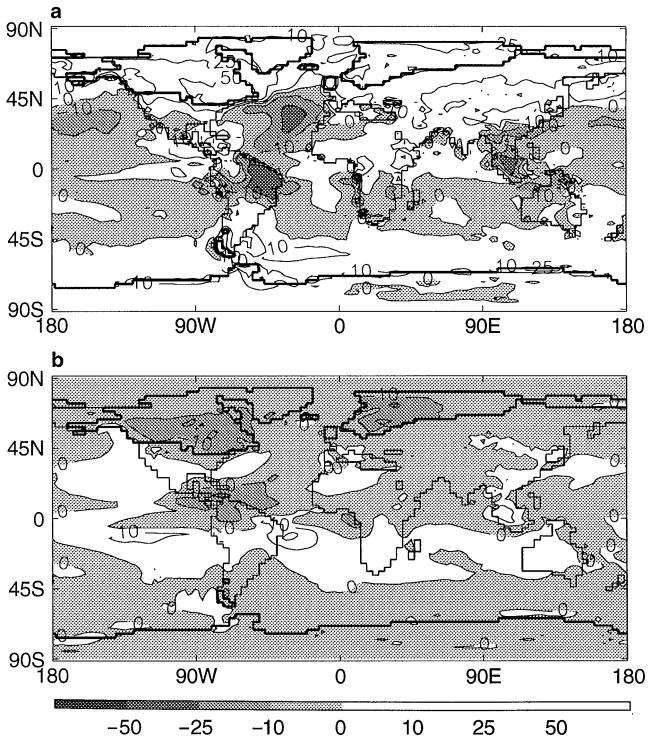

Fig. 6a, b. Change in annual average cloud radiative forcing, *areas of decreases shaded*, contours at 0, ± 10, 25, 50 Wm^{-2}. **a** Shortwave cloud forcing using *method a*; **b** longwave cloud forcing

the radiative forcing due to cloud changes from the surface albedo forcing. In this study four different methods are used (see Appendix) in an attempt to separate the contribution of changes in cloud and changes in surface albedo to the changes in cloud-radiative forcing. (Note that experiments simulating the effect of doubling atmospheric CO_2 concentrations will also include such surface albedo effects in their estimates of CRF, but these effects are generally ignored either on the assumption that they are small or because it is not known how to deal with them!).

The global mean change in SCF is substantially reduced if we try to remove the effect of increases in surface albedo (Appendix), leading to estimates of net cloud forcing which span zero (Table 6). Even with method c, which gives the largest correction, the residual change in SCF remains positive, indicating that changes in cloud tend to reduce the surface cooling and hence act as a negative feedback.

The local net affect of the simulated changes in cloud, even after allowing for changes in surface albedo, is to warm the ice sheets (Fig. 7) which represents a negative feedback offsetting the glacial cooling, and to cool the southern section of the Northern Hemisphere storm tracks, especially in the Atlantic, and much of the tropical North Atlantic and northeastern South America enhancing the glacial cooling, a positive feedback. In general, low cloud and cloud water content decrease where land ice and sea ice increase so that the reduction in reflection from clouds offsets the increased reflection of solar radiation from the surface. The cloud forcing is generally reduced over most of the continents, regardless of which method is used, which offsets the glacial cooling indicating that changes in cloud act as a negative feedback on temperature there.

5 Climate sensitivity

We are now in a position to be able to calculate the climate sensitivity parameter λ based on estimates derived from the LGM climate. Here we assume, as in previous studies, that the global mean temperature response can be simply related to the global mean forcing, and does not depend on the distribution of the forcing. Note that this may not necessarily be the case, as is discussed at the end of this section.

Palaeoclimatic data imply a global mean temperature change at the LGM compared to present to be in the region of -5 K. The best guess for the total global climate forcing during the ice age compared to the present was put at about -6.5 Wm^{-2} in Sect. 3. This value of ΔQ is similar to the estimates of Hansen et al. (1993) and Hoffert and Covey (1992) and is based on the combined forcings from the LGM reconstructions of ice sheet extents, greenhouse gas concentrations, glacial aerosol loading, vegetation changes, and insolation changes. These values for ΔQ and ΔT_{EQ} give a value of λ of 1.3 $Wm^{-2}K^{-1}$. If we use this value of λ and a ΔQ of 3.5 Wm^{-2} to represent the radiative forcing due to doubling atmospheric CO_2 from present day concentrations (as used in Sect. 3.2) then this would imply a global mean warming of 2.7 K on doubling CO_2.

By way of comparison, Hansen et al. (1993) estimate λ to be about 1.4 $Wm^{-2}K^{-1}$ (similar to the value above) from palaeoclimatic data, and ΔQ for doubling CO_2 to be 4.2 Wm^{-2}, giving an expected global mean warming of about 3 K on doubling CO_2 (Table 4). Hoffert and Covey (1992) have a higher estimate of λ of 2.2 $Wm^{-2}K^{-1}$ from palaeoclimatic data, and use a ΔQ for doubling CO_2 of 4.4 Wm^{-2}, giving an expected global warming of about 2 K on doubling CO_2. The Hoffert and Covey (1992) λ is higher because they assumed an ice age cooling of only 3 K which was calculated by averaging the CLIMAP SSTs and assuming that the temperature change over land was identical to that of the ocean in the same latitude zone. Hoffert and Covey state that this assumption is likely to be too conservative, and so the 5 K cooling of Hansen et al. (1993) may be a better estimate, and is more in line with GCM simulations.

An estimate of λ can also be made from the temperature response of the GCM used in this study. The total radiative forcing of -5.1 Wm^{-2} (-4.5 Wm^{-2} with the 'lost

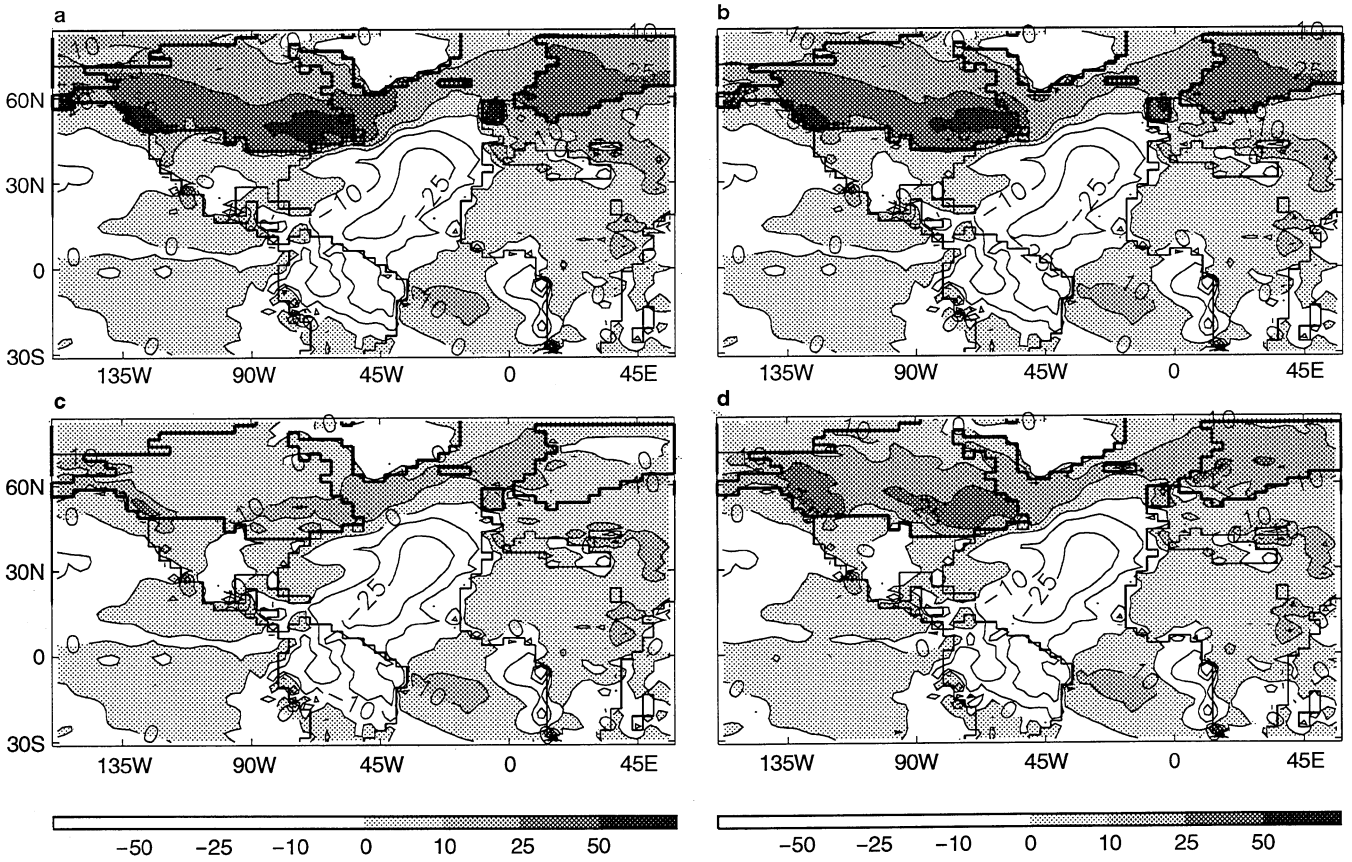

Fig. 7a–d. Change in annual average net cloud forcing using the four different methods for SCF. Contours at 0, ± 10, 25, 50 Wm^{-2}. Note that *positive values* have been *shaded*. **a** Using method a for SCF; **b** using *method b* for SCF; **c** using *method c* for SCF; **d** using *method d* for SCF

heat flux') produces a global mean temperature change of −4.9 K (− 4.4 K with the 'lost heat flux'). These values give a value of λ of just over 1.0 $Wm^{-2}K^{-1}$, and this would imply a global mean warming of 3.4 K on doubling CO_2. However, this model actually produces a $\Delta T_{2\times CO_2}$ of 2.9 K (Senior, personal communication), which is somewhat lower. The same calculations can be made using the results of Broccoli and Manabe (1987), although the published ice sheet forcing and CO_2 forcing are somewhat lower than expected and we apply some revisions to their estimates (see Table 4). The result is the same as found already, namely that the climate sensitivity to doubling present day CO_2, as deduced from the ice age simulation, is larger than that actually simulated by the model.

This implies that we may not be able to use the same estimate of λ as derived from the LGM simulation for the $2\times CO_2$ climate since nonlinear responses may complicate the estimation of ΔT from ΔF. For example, Oglesby and Saltzman (1990) found that the global temperature response to CO_2 concentration is nonlinear, with sensitivity decreasing as CO_2 increases; Hansen et al. (1997) found that changes in radiative forcing were most effective near the surface and in high latitudes; Spelman and Manabe (1984) found that the sea ice and snow albedo feedbacks become more important at lower temperatures and that the climate sensitivity increases as sea ice and snow extend to lower latitudes, consistent with the findings relating to vegetation changes in the work of Broccoli and Manabe (1987) who also point out that the geographical distribution of the forcing is important.

6 Summary and conclusions

The radiative forcing of the climate at the last glacial maximum has been investigated by performing a set of GCM experiments to isolate the effect of each of the ice age boundary conditions. These are a change to the surface albedo, changed insolation, and an estimate of the radiative forcing from lowering atmospheric carbon dioxide concentrations based on an experiment with doubled CO_2 concentrations. The largest forcing is the inclusion of the 21 kBP continental ice-sheets, but away from the ice sheets the lowering of CO_2 dominates. However, it is difficult to separate "forcings" from "response". For example, the simulated sea–ice response produces a significant radiative cooling, with a global mean radiative forcing of -0.8 Wm^{-2}. The sea ice could have been imposed as a boundary condition just as the continental ice-sheets were and would then have represented a radiative forcing, but in the experiments described here the sea ice is diagnosed by the model and therefore has been considered as a model response.

Considering the total LGM forcing to be a linear combination of the individual forcings derived from the set of GCM experiments, and including estimates for potential additional forcings such as increased atmospheric glacial aerosols, gives us a best guess of the forcing at 21 kBP to be of the order of $-6.5\ \mathrm{Wm}^{-2}$, which is slightly lower than the values reported by Hansen et al. (1993) and Hoffert and Covey (1992). Most of this difference is due to a higher greenhouse gas forcing in their studies.

The temperature response produced by each of the changed boundary conditions has also been investigated. Again, the largest response is due to the 21 kBP continental ice-sheets, and this cooling is dominated by the high albedo of the ice sheets and not by the increased elevation of the land. Locally, the sum of the temperature changes from the individual experiments is generally within one or two degrees of the total changes simulated in the LGM experiment, which indicates that the changes to the boundary conditions are fairly independent of one another. The simulated increases in sea ice enhance the cooling at the LGM giving a positive climate feedback. While the Northern Hemisphere forcing is dominated by the presence of the continental ice-sheets, the Southern Hemisphere forcing is dominated by the lowering of CO_2 and the cooling effect of the sea ice becomes more significant.

The climate sensitivity at the LGM can be calculated from the radiative forcing and the associated temperature change. Palaeoclimatic reconstructions can provide estimates of the temperature change and radiative forcing that has occurred in a climate that differed from the present and if we know the radiative forcing for a future climate then we can estimate the temperature change that will occur. Note however that this method does not give any regional details, merely global annual averages. Hoffert and Covey (1992) deduce that the global warming due to doubling CO_2 would be about 2 K and Hansen et al. (1993) deduce a warming of 3 K. The results from the HADSM2b GCM experiments imply a warming of 3.4 K using this method. This is higher than the 2.9 K actually simulated by this GCM in a doubled CO_2 experiment, and is probably because the albedo feedbacks are more effective at the lower glacial temperatures.

A detailed analysis of the cloud changes and how they influence the temperature response reveals that over the ice sheets the cloud changes represent a negative feedback on the climate tending to reduce the simulated glacial cooling. Large decreases in low-level high-albedo clouds over the ice sheets reduce the shortwave cooling by reflection, which outweighs the reductions in the longwave warming effect from reduced upper level cloud. However, large cloud changes occur where there are large changes to surface albedo, and the combined changes are not easily separated. Away from the ice sheets the forcing is dominated by the cloud increases over the North Atlantic and along parts of the ITCZ which represent a positive feedback on the climate in all four methods, enhancing the glacial cooling.

Finally, a comparison of the simulated SSTs to the CLIMAP data set produces some large-scale qualitative agreement, but several regional discrepancies which have been noted in other GCM results. An updated CLIMAP data set would be extremely useful now that more GCMs are including a representation of the oceanic mixed layer. Such models would benefit from a database with greater spatial coverage, and potentially more accurate estimates of palaeo-SSTs and sea–ice extent as a tool for validating and assessing the capabilites of the models in a climate change context, although this is more difficult for some regions such as the infertile subtropical gyres and deep basins where it is more difficult to obtain data.

Acknowledgements. This work was partially supported by the CEC under Contracts EV5V-CT94-0457 and ENV4-CT95-0075. We would like to thank Karl Taylor and Anthony Broccoli for their constructive, and complimentary, reviews; William Ingram for many useful suggestions particularly relating to the radiative forcing; Catherine Senior for her helpful comments and, along with James Murphy, lengthy discussions on "feedback analysis on shortware radiation changes"; and Mark Webb for advice on cloud radiative forcing.

Appendix

Shortwave cloud radiative forcing

We wish to determine the cloud feedback that arises from the change in the shortwave flux of radiation due to cloud changes alone (the *SCF*) with all other processes held fixed. The standard formalism for calculating a change in *SCF* is

$$\Delta SCF = SCF_{21\mathrm{k}} - SCF_{0\mathrm{k}} \qquad \textit{method a}$$

However, this can produce a cloud radiative forcing in the absence of any change in cloud if, as is the case in the experiments being dealt with in this study, there is a change in surface albedo or insolation.

We can attempt to limit the effect of albedo changes on *SCF* by rescaling using the ratio of the clear-sky co-albedos and the ratio of 21 kBP and 0 kBP insolation. One method would be to rescale using the present as the reference case:

$$\Delta SCF = SCF_{21\mathrm{k}}\left(\frac{1-\alpha_{CS0\mathrm{k}}}{1-\alpha_{CS21\mathrm{k}}}\frac{S_{0\mathrm{k}}}{S_{21\mathrm{k}}}\right) - SCF_{0\mathrm{k}} \qquad \textit{method b}$$

or alternatively use 21 kBP as the reference case:

$$\Delta SCF = SCF_{21\mathrm{k}} - SCF_{0\mathrm{k}}\left(\frac{1-\alpha_{CS21\mathrm{k}}}{1-\alpha_{CS0\mathrm{k}}}\frac{S_{21\mathrm{k}}}{S_{0\mathrm{k}}}\right) \qquad \textit{method c}$$

where $\alpha_{CS21\mathrm{k}}$ and $\alpha_{CS0\mathrm{k}}$ are the clear-sky planetary albedos at 21 kBP and 0 kBP respectively, and $S_{21\mathrm{k}}$ and $S_{0\mathrm{k}}$ are the insolation at 21 kBP and 0 kBP respectively. Both of these methods produce no change in *SCF* if there is no change in cloud, given a (realistic) change to the surface albedo or insolation.

The fourth approach used in this study is provided by Murphy (1995) who decomposes the changes in shortwave radiation at the top of the atmosphere into three components, changes in reflection to space by clouds (the component that we are interested in here), changes in surface albedo, and changes in the atmospheric absorption by water vapour and clouds. His formulation has been modified in this paper to allow for changes in insolation and this final method is referred to as *method d*.

Monthly mean data is used for all four methods with calculations performed at each grid-box before global annual mean values are calculated.

References

Berger AL (1978) Long-term variations of daily insolation and Quaternary climatic changes. J Atmos Sci 35 : 2362–2367

Broccoli AJ, Manabe S (1987) The influence of continental ice, atmospheric CO_2, and land albedo on the climate of the last glacial maximum. Clim Dyn 1 : 87–99

Broccoli AJ, Marciniak EP (1996) Comparing simulated glacial climate and paleodata: a reexamination. Paleoceanography 11 : 3–14

Bryan K (1969) Climate and the ocean circulation. III the ocean model. Mon Weather Rev 97 : 806–827

Burckle LH, Robinson D, Cooke D (1982) Reappraisal of sea–ice distribution in atlantic and pacific sectors of the southern ocean at 18,000 yr b.p. Nature 299 : 435–437

CLIMAP Project Members (1981) Seasonal reconstruction of the earth's surface at the last glacial maximum. Geological Society of America Map and Chart Series MC-36

COHMAP members (1988) Climatic changes of the last 18 000 years: observations and model simulations. Science 241 :1043–1052

Cullen MJP (1993) The unified forecast/climate model. Meteorol Mag 122 : 81–94

Dickinson RE (1986) How will climate change? In: Bolin B, Doos BR, Jaeger J, Warrick RA (eds) The greenhouse effect, climate change and ecosystems SCOPE Report 29, 206–270. John Wiley and Sons, Chichester, UK

Gates WL (1976) Modelling the ice-age climate. Science 191 : 1138–1144

Guilderson TP, Fairbanks RG, Rubenstone JL (1995) Tropical temperature variations since 20 000 years ago: modulating interhemispheric climate change. Science 263 : 663–665

Hall CD, Stratton RA, Gallani ML (1995) Climate simulations with the unified model: AMIP runs. Climate Research Technical Note 61, Hadley Centre Meteorological Office, London Road, Bracknell, UK

Hansen JE, Lacis A, Rind D, Russell L et al. (1984) Climate sensitivity analysis of feedback mechanisms. In: Hansen JE, Takahashi T (eds) Climate processes and climate sensitivity, Geophysical Monograph 29 130–163. American Geophysical Union Washington DC

Hansen JE, Lacis A, Ruedy R, Sato M, Wilson H (1993) How sensitive is the world's climate? Nat Geogr Res Explor 9 : 143–158

Hansen JE, Sato M, Ruedy R (1997) Radiative forcing and climate response. J Geophys Res (in press)

Hewitt CD, Mitchell JFB (1996a) GCM simulations of the climate of 6 kyr BP: mean changes and interdecadal variability. J Clim 9 : 3505–3529

Hewitt CD, Mitchell JFB (1996b) Palaeoclimate modelling intercomparison: UKMO GCM simulations for 6 kBP and 21 kBP. Climate Research Technical Note 72, Hadley Centre Meteorological Office, London Rd, Bracknell, UK

Hibler WD (1979) A dynamic-thermodynamic sea ice model. J Phys Oceanogr 9 : 815–846

Hoffert MI, Covey C (1992) Deriving global climate sensitivity from palaeoclimate reconstructions. Nature 360 : 573–576

Houghton JT, Meira Filho LG, Callender BA, Harris N, Kattenberg A, Maskell K (1995) Climate change 1995 – the science of climate change. Cambridge University Press, Cambridge, 572 pp

Johns TC, Carnell RE, Crossley JF, Gregory JM, Mitchell JFB, Senior CA, Tett SFB, Wood RA (1997) The second Hadley Centre coupled ocean-atmosphere GCM: Model description, spinup and validation. Clim Dyn 13 : 103–134

Joussaume S, Taylor KE (1995) Status of the Paleoclimate Modeling Intercomparison Project. In: Proceedings of the first international AMIP scientific conference WCRP-92 425–430 Monterey, USA

Kutzbach JE, Guetter PJ (1986) The influence of changing orbital parameters and surface boundary conditions on climate simulations for the past 18 000 years. J Atmos Sci 43 : 1726–1759

Lautenschlager M, Herterich K (1990) Atmospheric response to ice age conditions: climatology near the earth's surface. J Geophys Res 95 : 22547–22557

Manabe S, Broccoli AJ (1985a) A comparison of climate model sensitivity with data from the last glacial maximum. J Atmos Sci 42 : 2643–2651

Manabe S, Broccoli AJ (1985b) The influence of continental ice sheets on the climate of an ice age. J Geophys Res 90 : 2167–2190

Mitchell JFB, Johns TC, Gregory JM, Tett SFB (1995) Climate response to increasing levels of greenhouse gases and sulphate aerosols. Nature 376 : 501–504

Murphy JM (1995) Transient response of the Hadley Centre coupled ocean-atmosphere model to increasing carbon dioxide: Part III. Analysis of global-mean response using simple models. J Clim 8 : 496–514

Oglesby RJ, Saltzman B (1990) Sensitivity of the equilibrium surface temperature of a GCM to systematic changes in atmospheric carbon dioxide. Geophys Res 17 : 1089–1092

Ramanathan V, Cess RD, Harrison EF, Minnis P, Barkstrom BR, Ahmad E, Hartmann D (1989) Cloud-radiative forcing and climte: results from the Earth radiation budget experiment. Science 243 : 57–63

Schneider SH (1975) On the carbon dioxide – climate confusion. J Atmos Sci 32 : 2060–2066

Semtner AJ (1976) A model for the thermodynamic growth of sea ice in numerical investigations of climate. J Phys Oceanogr 6 : 379–389

Senior CA, Mitchell JFB (1993) Carbon dioxide and climate: the impact of cloud parametrization. J Clim 6 : 393–418

Simmons AJ, Burridge DM (1981) An energy and angular momentum conserving finite difference scheme with hybrid coordinates. Mon Weather Rev 109 : 758–766

Spelman MJ, Manabe S (1984) Influence of oceanic heat transport upon the sensitivity of a model climate. J Geophys Res 89 : 571–586

Tushingham AM, Peltier W (1991) ICE-3G: a new global model of late Pleistocene glaciation based upon geophysical predictions of post-glacial relative sea level change. J Geophys Res 96 : 4497–4523